University of Groningen

Radiogenomic Models Using Machine Learning Techniques to Predict EGFR Mutations in Non-Small Cell Lung Cancer

Nair, Jay Kumar Raghavan; Saeed, Umar Abid; McDougall, Connor C; Sabri, Ali; Kovacina, Bojan; Raidu, B V S; Khokhar, Riaz Ahmed; Probst, Stephan; Hirsh, Vera; Chankowsky, Jeffrey

IMPORTANT NOTE: You are advised to consult the publisher's version (publisher's PDF) if you wish to cite from it. Please check the document version below.

Document Version
Publisher's PDF, also known as Version of record

Publication date:
2021

[Link to publication in University of Groningen/UMCG research database](#)

Citation for published version (APA):
Nair, J. K. R., Saeed, U. A., McDougall, C. C., Sabri, A., Kovacina, B., Raidu, B. V. S., Khokhar, R. A., Probst, S., Hirsh, V., Chankowsky, J., Van Kempen, L. C., & Taylor, J. (2021). Radiogenomic Models Using Machine Learning Techniques to Predict EGFR Mutations in Non-Small Cell Lung Cancer. *Canadian association of radiologists journal-Journal de l association canadienne des radiologistes*, *72*(1), 109-119. https://doi.org/10.1177/0846537119899526

Artificial Intelligence / Intelligence artificielle

Radiogenomic Models Using Machine Learning Techniques to Predict EGFR Mutations in Non-Small Cell Lung Cancer

Jay Kumar Raghavan Nair, MD[1,2,3] , Umar Abid Saeed, MD[1,3],
Connor C. McDougall, MSc[4], Ali Sabri, MD, Mmed, FRCPC[5,6],
Bojan Kovacina, MD, CM, FRCPC[6], B. V. S. Raidu, MSc[7],
Riaz Ahmed Khokhar, MS[1,8], Stephan Probst, MD[9],
Vera Hirsh, MD, FRCPC[10], Chankowsky Jeffrey, MD, CM, FRCPC[1],
Léon C. Van Kempen, MD[11,12], and Jana Taylor, MD, CM, FRCPC[1]

Abstract
Background: The purpose of this study was to build radiogenomics models from texture signatures derived from computed tomography (CT) and ^{18}F-FDG PET-CT (FDG PET-CT) images of non-small cell lung cancer (NSCLC) with and without epidermal growth factor receptor (*EGFR*) mutations. **Methods:** Fifty patients diagnosed with NSCLC between 2011 and 2015 and with known *EGFR* mutation status were retrospectively identified. Texture features extracted from pretreatment CT and FDG PET-CT images by manual contouring of the primary tumor were used to develop multivariate logistic regression (LR) models to predict *EGFR* mutations in exon 19 and exon 20. **Results:** An LR model evaluating FDG PET-texture features was able to differentiate *EGFR* mutant from wild type with an area under the curve (AUC), sensitivity, specificity, and accuracy of 0.87, 0.76, 0.66, and 0.71, respectively. The model derived from CT texture features had an AUC, sensitivity, specificity, and accuracy of 0.83, 0.84, 0.73, and 0.78, respectively. FDG PET-texture features that could discriminate between mutations in *EGFR* exon 19 and 21 demonstrated AUC, sensitivity, specificity, and accuracy of 0.86, 0.84, 0.73, and 0.78, respectively. Based on CT texture features, the AUC, sensitivity, specificity, and accuracy were 0.75, 0.81, 0.69, and 0.75, respectively. **Conclusion:** Non-small cell lung cancer texture analysis using FGD-PET and CT images can identify tumors with mutations in *EGFR*. Imaging signatures could be valuable for pretreatment assessment and prognosis in precision therapy.

Résumé
Contexte : L'objectif de cette étude était de construire des modèles de radiogénomique à partir des signatures texturales dérivées de clichés acquis par tomodensitométrie (TDM) et tomographie par émission de positons couplée à la tomodensitométrie au fluorodésoxyglucose (TEP/TDM 18-FDG) de cancer du poumon non à petites cellules (CPNPC), avec ou sans mutation du récepteur du facteur de croissance épidermique (EGFR). **Méthodes :** Cinquante patients porteurs d'un diagnostic de CPNPC entre 2011 et 2015 et d'une mutation de l'EGFR ont été identifiés de manière rétrospective. Les caractéristiques

[1] Department of Radiology, McGill University Health Centre, Montreal, Québec, Canada
[2] Department of Radiology, McMaster University Faculty of Health Sciences, Hamilton, Ontario, Canada
[3] Department of Radiology, University of Calgary, Calgary, Alberta, Canada
[4] Department of Mechanical Engineering, University of Calgary, Calgary, Alberta, Canada
[5] Department of Radiology, McMaster University, Hamilton, Ontario, Canada
[6] Department of Radiology, Jewish General Hospital, Montreal, Québec, Canada
[7] Raidu Analysts and Associates, Mumbai, India
[8] Department of Surgery, Khokhar Medical Centre, Rawalpindi, Pakistan
[9] Department of Nuclear Medicine, Jewish General Hospital, Québec, Montreal, Canada
[10] Department of Oncology, McGill University Health Centre, Montreal, Québec, Canada
[11] Department of Pathology, University Medical Center Groningen, University of Groningen, Groningen, the Netherlands
[12] Department of Pathology, Jewish General Hospital, Montreal, Québec, Canada

Corresponding Author:
Jay Kumar Raghavan Nair, Department of Radiology, Montreal General Hospital, McGill University, 1650 Cedar Ave, Montreal, Québec, Canada H3G 1A4.
Email: jay_drishti@yahoo.com

texturales extraites des clichés de TDM et de TEP/TDM 18-FDG avant traitement par tracé manuel des contours des tumeurs primaires ont été exploitées pour mettre au point des modèles de régression logistique (RL) multivariés afin de prédire les mutations des exons 19 et 21 du gène codant pour l'EGFR. **Résultats :** Un modèle LR d'analyse des caractéristiques texturales de TEP/TDM 18-FDG a permis de différencier les mutants de l'EGFR des types sauvages avec une aire sous la courbe (ASC), une sensibilité, une spécificité et une précision de respectivement 0,87, 0,76, 0,66 et 0,71. Le modèle dérivé des caractéristiques texturales de la TDM présentait une ASC, une sensibilité, une spécificité et une précision de respectivement 0,83, 0,84, 0,73 et 0,78. Les caractéristiques texturales de TEP/TDM 18-FDG pouvant discriminer les mutations de l'exon 19 et de l'exon 21 de l'EGFR arboraient une ASC, une sensibilité, une spécificité et une précision de respectivement 0,86, 0,84, 0,73 et 0,78. Selon les caractéristiques texturales de la TDM, l'ASC, la sensibilité, la spécificité et la précision étaient respectivement de 0,75, 0,81, 0,69 et 0,75. **Conclusion :** L'analyse de la texture du cancer du poumon non à petites cellules (CPNPC) sur des clichés acquis par TEP/TDM 18-FDG et TDM peut permettre d'identifier les tumeurs porteuses de mutations du gène de l'EGFR. Les signatures inhérentes aux clichés d'imagerie pourraient constituer de précieux outils pour l'examen préthérapeutique et le pronostic lors de l'établissement d'un traitement de précision.

Introduction

Lung cancer remains the leading cause of cancer deaths both men and women in Canada. Non-small cell lung cancers (NSCLCs) account for 85% to 90% of all lung cancer cases.[1] Conventional management of NSCLC involves resection of the tumor, followed by chemotherapy, radiotherapy, or combination therapy if surgical resection is not feasible.[2] Prognosis is usually dependent on the stage of the disease at the time of the diagnosis. However, it has been increasingly observed that patients with same stage of the disease have different outcomes. Different driver mutations have been identified in NSCLC, including oncogenic mutations in epidermal growth factor receptor (*EGFR*), *BRAF*, *ROS1*, *MET*, and *ALK*.[3] Epidermal growth factor receptor mutations are more frequently detected in never smokers, and the frequency of *EGFR*-mutated NSCLC has been shown to correlate with the ethnicity of the patient.[4] Landmark clinical trials have demonstrated that patients with these mutations treated with targeted biological therapies such as tyrosine kinase inhibitors had a better progression-free survival, better tolerance to therapy, and quality of life than those patients treated with placebo or conventional chemotherapies.[5-10] Deletions within exon 19 and mutations in exon 21 have been shown to be the most frequent EGFR-TKI (tyrosine kinase inhibitors) sensitive mutations (80%) in NSCLC.[11]

Detection of the activating mutation in driver mutations for the selection of a targeted therapy requires DNA analysis of a tumor biopsy. However, a representative tissue sample cannot always be obtained because the tumor cannot always be biopsied. Also, random sampling does not always allow for adequate assessment of the phenotypic or genetic variation within a tumor, due to tumor heterogeneity[12] Potentially, a liquid biopsy could be obtained to determine mutations in plasma. But, as demonstrated for *EGFR*, mutations can be missed when the tumor is small and may not shed a sufficient amount of DNA in the plasma circulation.[13] Potential alternative non-invasive methods which could aid in targeted treatment planning for lung cancer patients are needed. Cross-sectional imaging facilitates evaluation of the entire lesion, compared to the targeted segment of the lesion on needle biopsy. However, studies demonstrating the relationship between morphological/qualitative computed tomography (CT) scan features of the tumor and the presence/absence of *EGFR* mutations, based on semantic features that demonstrate interobserver variability.[14-16] Therefore, there is a need for a robust quantitative model to predict *EGFR* mutations in exon 19 and 21 in NSCLC lung cancer patients.

Radiomics refers to the extraction and analysis of quantitative imaging features with high output from medical images obtained from CT, positron emission tomography, or magnetic resonance imaging.[17] Radiogenomics is the combination of radiomic features with genomic data.[18] We hypothesize that using texture signatures from CT and 18F-FDGPET features can differentiate between lung cancer with wild-type *EGFR* and exon 19- or exon 21-mutated *EGFR*. The goal of this study is to develop an image texture biomarker for the detection of different *EGFR* mutations.

Materials and Methods

Patient Selection

A retrospective chart review of 80 patients with lung cancer diagnosed and treated at our institution, between 2011 and 2015 was performed. Fifty patients were identified who had biopsy-proven NSCLC, pretreatment contrast-enhanced CT and FDG PET-CT of the chest, and known EGFR mutation status. Exclusion criteria included patients with small primary tumors (less than 5 mm in maximum diameter), significant air bronchograms, and breathing artifacts, which would have precluded accurate texture analysis (Figure 1). Approval from the local institution's research ethics board was obtained which waived off informed consent (MM-CODIM-MBM-CR15-53).
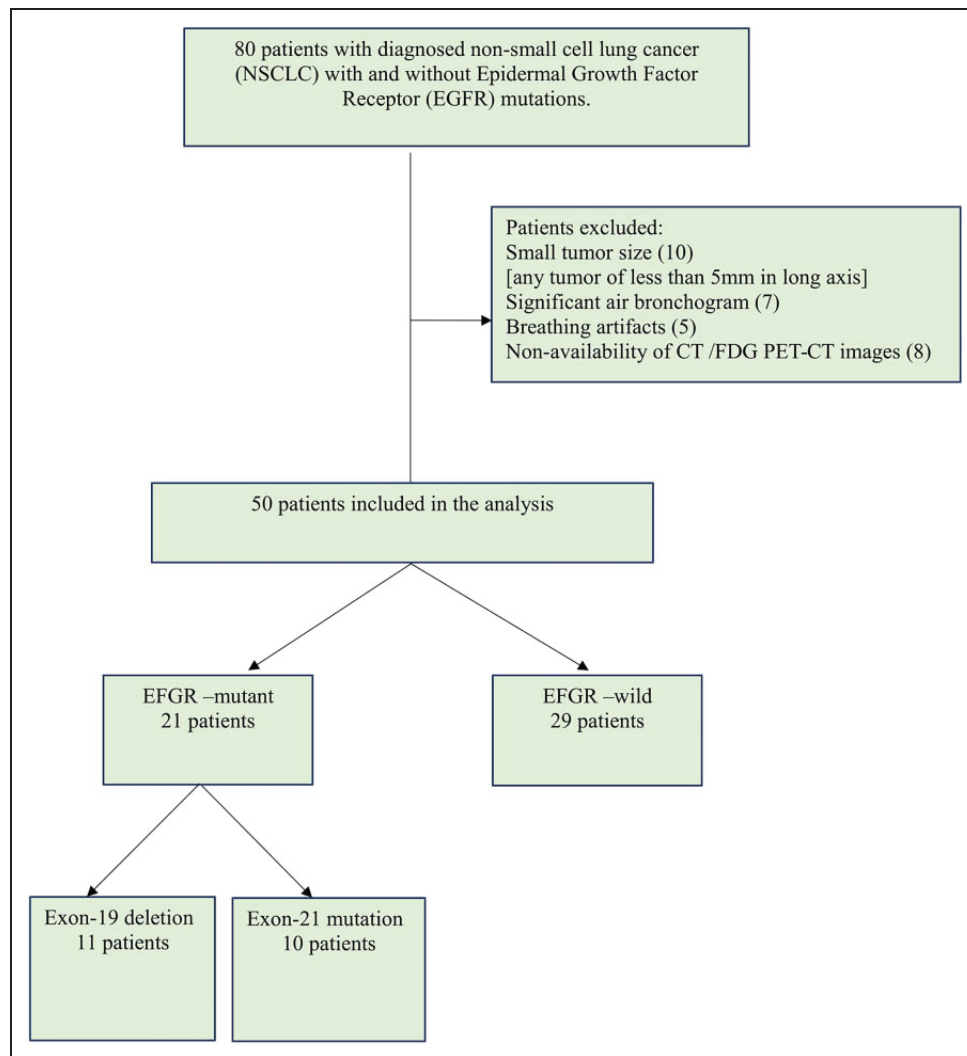
Figure 1. Flowchart of patients.

Imaging Acquisition and Segmentation

Contrast-enhanced CT and 18F-FDG PET-CT of the chest were performed according to standard oncology protocol of the institution. All scans of the chest were obtained using one of the following CT scanners: Lightspeed VCT 64-slice or 16-slice CT scanners (GE Healthcare, Milwaukee, Wisconsin), Revolution 64-slice CT scanner (GE Healthcare), and Somatom128-slice CT scanner (Siemens Healthcare, Forchheim, Germany). The examinations were obtained in inspiration, 30 seconds after administration of 60 ml of non-ionic iodinated contrast material (Omnipaque300 I/mL; GE Healthcare, Princeton, NJ) at the rate of 2 mL/s and covered the region from the lung apices to the adrenal glands. FDG PET-CT was performed on a single GE Discovery ST hybrid PET/CT scanner; images were obtained approximately 60 to 90 minutes following 15 mCi of intravenous injection of FDG. We employed a compensation method to correct for the variations of radiomic features caused by using different CT scanners and reconstruction techniques.[19]

Using the reformatted soft tissue algorithm contrast-enhanced CT axial images with 5-mm slice thickness and transverse FDG PET-CT images containing SUV > 2.5, contours defining 3D tumor regions for each patient were manually drawn slice-by-slice on both CT and FDG PET-CT images by Thoracic imaging fellows (J.K.R.N.) and (U.A.S.) working in consensus. Contouring was then validated for each segmented region of interest, independently by fellowship-trained Thoracic radiologist (J.T). Contouring was done using OsiriX (Pixmeo SARL, Geneva, Switzerland) software.[20] Both OsiriX and DICOM Anonymizer Pro were run on an iMac 27″ 4.0 GHz IntelCorei7 with Retina 5k display. Figure 2 demonstrates representative images of segmentation.

Standardization of Molecular Testing

Tissue for histopathological examination was obtained using endobronchial ultrasound–guided needle biopsy from 38
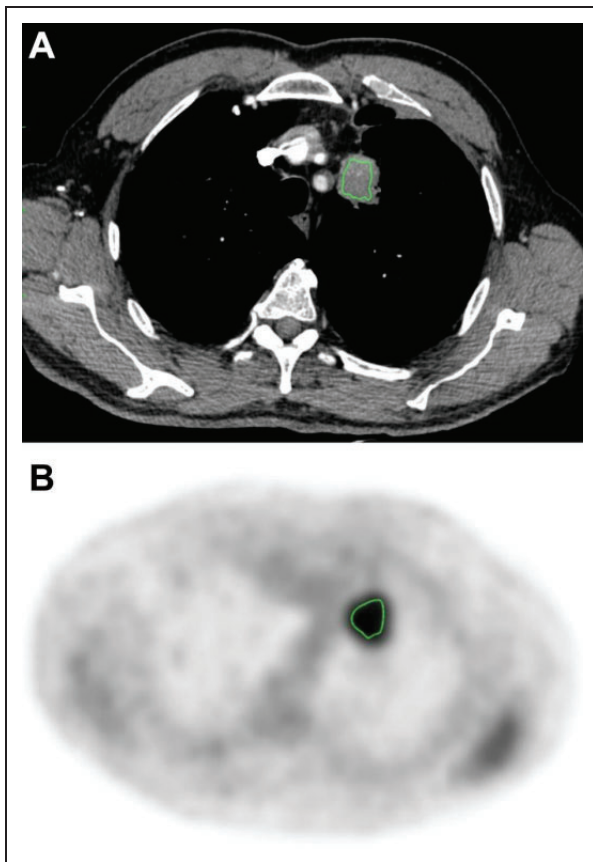
Figure 2. Representative segmentation images for texture analysis. Segmented contrast-enhanced axial CT (A) and Axial FDG PET-CT (B) images of the left upper lobe lung mass in a 65-year-old male. CT, computed tomography.

patients and surgically resected specimens from 12 patients. Studies comparing EGFR mutation status of biopsies and resection specimens have demonstrated high concordance between the presence of an EGFR exon 19 deletion or L858R mutation in the biopsy and surgical resection specimen.[21-23] Recent guidelines on molecular testing in NSCLC by College of American Pathologists (CAP)/International Association for the Study of Lung Cancer/Association recommend that *EGFR* testing of multiple different areas within a single tumor is unnecessary.[24]

Histological examination of hematoxylin and eosin–stained slides derived from formalin fixed and paraffin embedded (FFPE) lung samples was performed by expert pathologists to verify the diagnosis and to assess the adequacy of the tissue for the study. No retrospective slide review was performed. Tumor tissue was then manually macrodissected from unstained sections. A Cobas DNA Sample preparation kit (Roche, Risch-Rotkreuz, Switzerland) was used to manually isolate DNA from FFPE. DNA was quantified and stored at $-4°C$. *EGFR* mutation analysis was performed with the Cobas *EGFR* mutation test v2 (Roche) according to the supplier's instructions. All tests were performed in a routine diagnostic setting in a CAP/CLIA compliant laboratory.

Texture Features

Each contour was imported into in-house-developed Matlab texture-feature software for texture analysis. Texture features (326) were extracted from the contoured primary tumor on CT and FDG PET-CT images. These features can be classified into 3 separate sets: (1) first-order statistics (34 features), (2) volume-based statistics (6 features), and (3) higher order statistical textural information (286 features).

First-order statistics are calculated from all voxels in the region of interest and represent common measurements such as mean and standard deviation, among others. Volume-based features quantify the size and shape of the region of interest. Texture features are a broad spectrum of higher order statistical operations that characterize the heterogeneity of the region in 3 dimensions.

Not all 326 features were included in the machine learning models implemented later in this manuscript. Linear discriminant analysis (LDA) was implemented to reduce the large set of statistical features to a subset of the most significant features, by ranking the features in order of their discriminative importance. This was done in to minimize overfitting problems. These features (Appendix A) were then used to train a machine learning algorithm to classify the desired binary groups.

Machine Learning Model

Top ranking texture features were computed in 100 bootstrap training sets and then incorporated into multivariate logistic regression (LR) model for prediction of EGFR status and subtype of exon deletion using the equation:

$$P(y_i = 1/x_i) = \frac{\exp[g(x_i)]}{1 + \exp[g(x_i)]} \quad g(x_1) = \beta_0 + \sum_{j=1}^{p} \beta_j x_{ij}$$

for $i = 1, 2 \ldots \ldots \ldots, N$.

The first portion of the equation is the LR function which was simplified by transforming it into a log function by derivation.

P is the probability of the outcome status, i is the number of patients, x_i is the texture parameter (independent variable), $g(x_1)$ is the dependent variable which determines probability of the outcome status, β_0 is the constant for each texture parameter (slope), p is the total number of parameters, and j is the parameter number.

Logistic regression is often used in small data sets due to their resistivity to overfitting. Due to the small sample size of our study, LR minimized overfitting and provided reliable cross-validated accuracy and area under the curve (AUC). In our study, LR was implemented to discriminate between 4 binary groups. For each binary group, the data sets were trained with increasing numbers of texture features, determined by LDA. The optimal number of features was determined by varying the number of features included in the LR model until

cross-validated accuracy was maximized. Due to the asymmetry between the positive and negative binary groups, a correction was required to ensure the models were not biased toward a certain binary subset. This was corrected by oversampling each group to equalize the positive and negative subclasses.

Receiver Operating Characteristic Analysis and Leave-One-Out Cross-Validation

Receiver operating characteristic (ROC) curves were produced for each texture feature threshold. The AUC of an ROC curve was used to evaluate quality and performance of the derived machine learning model. However, this method often cannot detect overfitting, especially in small data sets. When overfitting occurs, the model classifies the training data set well but cannot be applied to new data sets. Therefore, to minimize overfitting, the leave-one-out cross-validation (LOOCV) approach was performed to train the models. The LOOCV model analyzes the data with one less than the total patient population. Then, the patient left out of the training group is tested with the fitted model to determine whether it can accurately classify the patient into the correct binary class. This is completed for all patients in the data set, "leaving one out" for each iteration. The accuracy was then calculated considering results from all iterations. This accuracy tests the variance in the model by assessing overfitting. This was the primary statistic used when determining a texture feature dimensionality threshold.

Multiple Methodology Points and STARD Guidelines

The study was designed to meet the "Standards for Reporting Diagnostic Accuracy Studies" (STARD) guidelines. Multiple statistics were generated in the current work (sensitivity, specificity, accuracy, and AUC) to assess the performance of texture image analysis technique. The tests were compared with a reference standard (needle biopsy/surgical resection) to assess performance. The reference standard has been described in the paragraph on standardization of molecular testing. The performance statistics were optimized using a test positivity cutoff by completing an ROC analysis. In addition, the performance statistics were assessed using a cross-validation technique that has been used in the literature and complies with the STARD standards.[25] Confidence intervals for each performance statistic were reported to display the associated uncertainty in the analysis. A DeLong AUC comparative test was completed between the 2 techniques attempted in the current study, which was used to determine whether the results from the 2 techniques were statistically distinct.[26]

Results

A total of 50 patients, 32 males and 18 females, with NSCLC who met the selection criteria, were included in the analysis. Twenty-one patients had an *EGFR* mutation. For 29 patients, no *EGFR* mutation was identified in *EGFR* and was classified

Table 1. Patient Characteristics.

Factor	Number	Percentage
Sex		
Male	32	64%
Female	18	35%
Smoking		
Current smoker	10	20%
Former smoker	25	50%
Nonsmoker	15	30%
EGFR mutation		
Negative	29	58%
Positive	21	42%
Exon 19 deletion	11	52%
Exon 21 mutation	10	48%

Abbreviation: EGFR, epidermal growth factor receptor.

Table 2. Top 10 Selected Features for EGFR-Mutant and Wild-Type Groups.

Texture Features	Top-Ranked Features
CT Texture Features	NGTDM_600_Complexity
	GLRL_Saggital_30_ShortRunEmphasis
	GLRL_Saggital_30_ShortRunHighGrayLevelEmphasis
	GLRL_Saggital_120_ShortRunHighGrayLevelEmphasis
	GLRL_Coronal_120_ShortRunHighGrayLevelEmphasis
	GLRL_Coronal_30_ShortRunEmphasis
	GLRL_Saggital_120_ShortRunEmphasis
	GLRL_Axial_30_ShortRunEmphasis
	GLRL_Coronal_120_ShortRunEmphasis
	FirstOrder_HistogramBin2
PET-CT Texture Features	NGTDM_600_Complexity
	GLRL_Saggital_30_ShortRunEmphasis
	GLRL_Saggital_30_ShortRunHighGrayLevelEmphasis
	GLRL_Saggital_120_ShortRunHighGrayLevelEmphasis
	GLRL_Coronal_120_ShortRunHighGrayLevelEmphasis
	GLRL_Coronal_30_ShortRunEmphasis
	GLRL_Saggital_120_ShortRunEmphasis
	GLRL_Axial_30_ShortRunEmphasis
	GLRL_Coronal_120_ShortRunEmphasis
	FirstOrder_HistogramBin2

Abbreviations: CT, computed tomography; EGFR, epidermal growth factor receptor.

as wild type. Among the *EGFR* mutation-positive cases, 11 cases had an exon 19 deletion and 10 cases had an exon 21 mutation. Patient characteristics are summarized in Table 1.

The patients were divided into 4 binary groups, 2 binary groups (1 each for CT and for FDG PET-CT) to determine *EGFR*-mutant and wild types and other 2 binary groups (one each for CT and for FDG PET-CT) to differentiate between exon 19-deleted and exon 21-mutated *EGFR* using texture features and machine learning models.

Linear discrimination analysis was used to rank each texture feature individually in terms of its discriminatory importance. The top 10 most distinctive texture features for *EGFR* mutant versus wild-type binary groups are listed in Table 2,

while the top 4 most distinctive texture features mutation on exon 19 deleted versus exon 21-mutated *EGFR* mutant patients are listed in Table 3. As detailed in the methodology,

Table 3. Top 4 Selected Features for Exon 19-Deleted and Exon 21-Mutated *EGFR*.

Texture Features	Top-Ranked Features
CT Texture Features	GLCM_coronal_NL60_corrm_m
	GLCM_saggital_NL60_corrm_m
	GLCM_saggital_NL60_contr_m
	GLCM_coronal_NL60_contr_m
PET-CT Texture Features	LBP_Hist4_5
	LBP_Mean_5
	LBP_Hist6_3
	LBP_Hist5_5

Abbreviations: CT, computed tomography; EGFR, epidermal growth factor receptor.

the maximum number of texture features included was determined by maximizing cross-validated accuracy. This value was not the same for each binary group or each machine learning model. To make one-to-one comparisons, the average threshold was determined for all models/binary groups. This threshold was 10 ± 2 texture features for *EGFR* and 4 ± 1 texture features for mutation-specific subsets, where the error was determined from the standard deviation of all thresholds averaged. This standard deviation was converted into uncertainty when reporting AUCs and cross-validated accuracies.

Logistic regression was used as a machine learning model to discriminate between the various binary groups. For the *EFGR* mutant versus wild type, AUC of the model derived from FDG PET-CT texture features measured 0.8713 ± 0.05, slightly more than 0.8307 ± 0.07 for the model derived from CT texture features (Figures 3 and 4). We then proceeded to
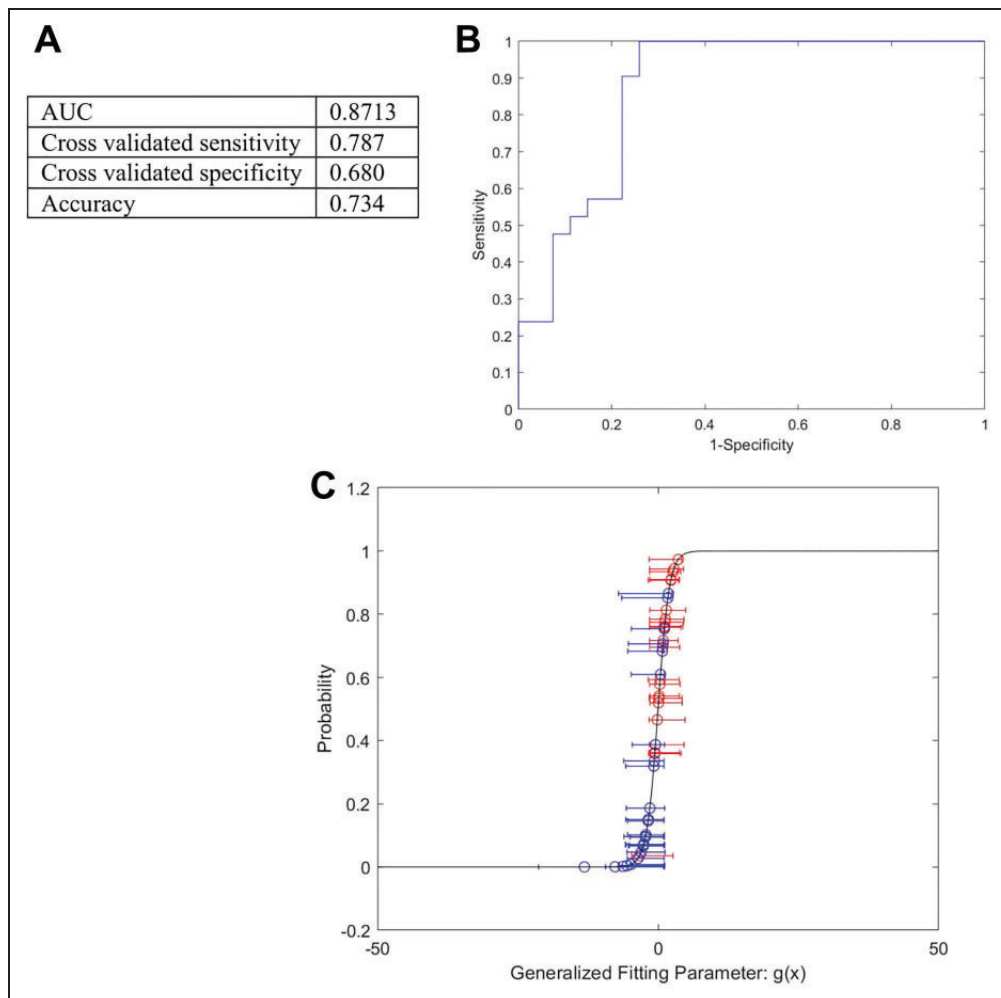

Figure 3. *EGFR* mutation status using PET-CT Texture features. A, Tabulated results for the prediction of EGFR mutations with texture features derived from PET-CT images. B, Corresponding receiver operator characteristic curve. C, Final multivariable logistic regression (PET-CT) model for EGFR status. Blue dots correspond to EGFR mutation-negative status, while red dots imply EGFR mutation-positive status. Error bars represent the standard deviation of the multivariable model response for each patient over all 100 bootstrap samples, on a 95% confidence interval. EGFR indicates epidermal growth factor receptor. CT, computed tomography; EGFR, epidermal growth factor receptor.
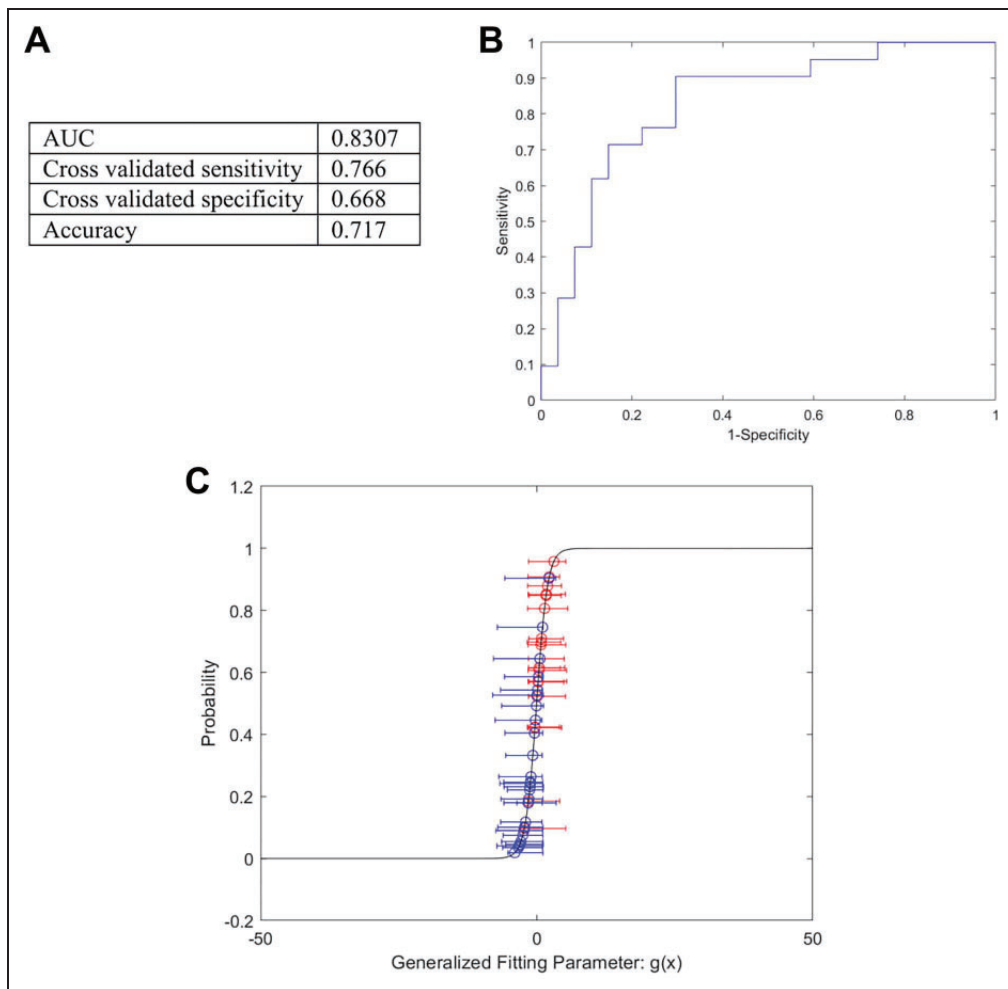
Figure 4. EGFR mutation status using CT Texture features. A, Tabulated results for the prediction of EGFR mutations with texture features derived from CT images. B, Corresponding receiver operator characteristic curve. C, Final multivariable logistic regression (CT) model for EGFR status. Blue dots correspond to EGFR mutation-negative status, while red dots imply EGFR mutation-positive status. Error bars represent the standard deviation of the multivariable model response for each patient over all 100 bootstrap samples, on a 95% confidence interval. CT, computed tomography; EGFR, epidermal growth factor receptor.

analyze radiomics features of the specific mutations within the *EGFR* mutant group. In this subgroup also, AUC of the model derived from FDG PET-CT texture features measured 0.860 ± 0.07 and was higher than to 0.750 ± 0.04 for the model derived from CT texture features (Figures 5 and 6). Thus, texture features derived from FDG PET-CT imaging had higher AUC compared to CT, both for identification of *EGFR* mutation and for differentiating between the mutations in exon 19 and 21. A DeLong AUC test was also completed to compare the AUCs of 2 ROC analyses and determine whether one is statistically better than the other.[26] This analysis determined the differences between PET/CT and CT results were not significant ($P > .05$). However, the trend pointing toward PET/CT is promising but was limited by the small data set to statistically determine whether PET/CT is better than CT. For both PET/CT and CT cases, the AUCs calculated indicate the methodology achieves high diagnostic accuracy.

Discussion

In our study, quantitative texture features were extracted from CT and FDG PET-CT images from NSCLC were analyzed and correlated with *EGFR* mutation status. Additional prediction models were developed, one each for FDG PET-CT and CT to distinguish between *EGFR* mutations in exons 19 and 21. Texture features derived from FDG PET-CT imaging had higher AUC compared to those derived from CT for identification and distinction of the *EGFR* mutations. It can be argued that this difference may be related to better tumor segmentation on FDG PET-CT scans as the FDG avid areas are confined to the bulk of the tumor. In addition, on CT images, despite all efforts to accurately contour the lesions, some extra-tumoral tissue consisting of consolidated/atelectatic lung may have been segmented out along with the tumor.

Several studies have previously demonstrated the potential ability of morphological imaging characteristics to detect
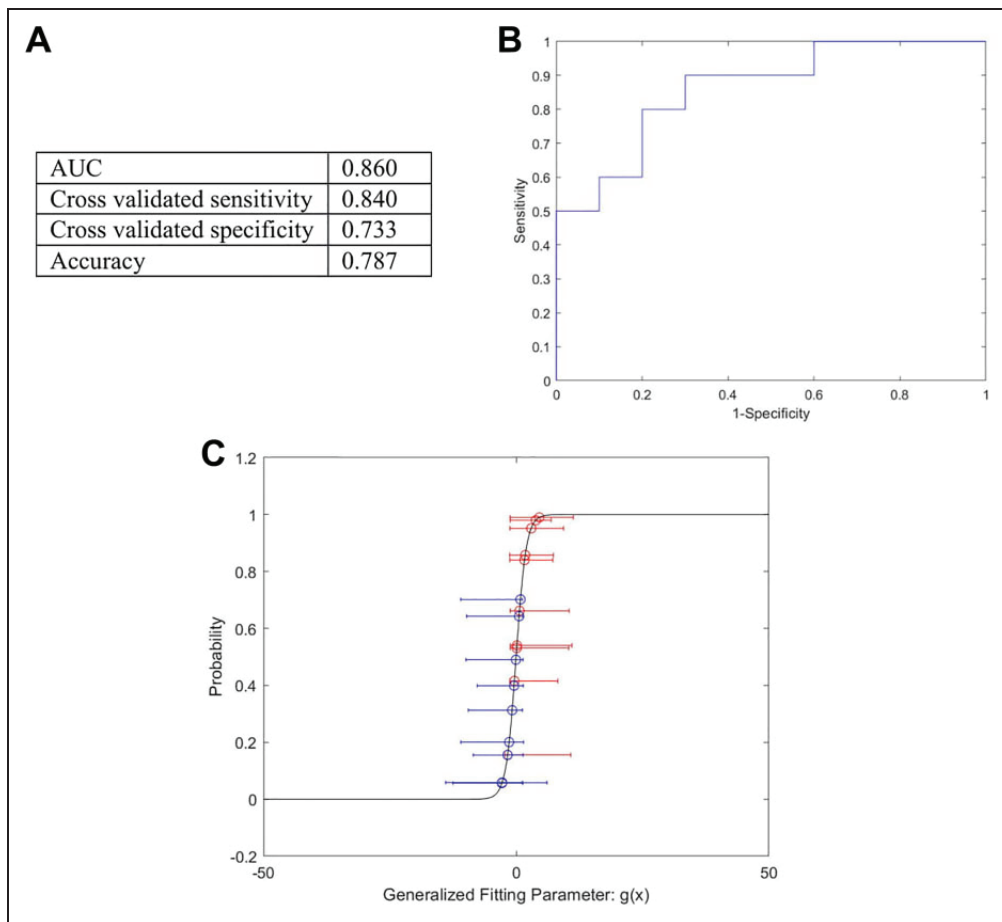
Figure 5. Comparison of imitations in EGFR exon 19 and 21 in EGFR mutant-positive patients using PET-CT Texture features. A, Tabulated results for the prediction of mutations in EGFR exon 19 and 21 with texture features derived from PET-CT images. B, Corresponding receiver operator characteristic curve. C, Final multivariable logistic regression (PET-CT) model for point mutations in EGFR exon 19 and 21 in EGFR mutant-positive patients. Blue dots correspond to mutation on EGFR exon 21, while red dots imply deletions in EGFR exon 19. Error bars represent the standard deviation of the multivariable model response for each patient over all 100 bootstrap samples, on a 95% confidence interval. CT, computed tomography; EGFR, epidermal growth factor receptor.

the presence/absence of clinically significant mutations from CT[27-32] and FDGPET-CT images.[33] Chen et al showed that conventional CT features, including emphysema, degree of primary tumor lobulation, lymph node size, and status facilitated in predicting the presence of *EGFR* mutations in advanced pulmonary adenocarcinoma.[28] Similarly, a systematic review and meta-analysis of CT morphology and clinical characteristics that predict the risk of *EGFR* mutation in NSCLC corroborated that the presence of ground glass opacity (GGO), air bronchogram, pleural retraction, and vascular convergence were significant risk factors of *EGFR* mutation in NSCLC.[32] These studies only addressed qualitative semantic features that correlate with the presence of an *EGFR* mutation. The process of semantic feature annotation is operator-dependent with significant inter-observer variability. Furthermore, features to quantify tumoral heterogeneity were not considered.

To the best of our knowledge, our study is the first to compare radiomics features extracted from CT and FGD PET-CT images for the identification of specific *EGFR* mutations in

NSCLC. This study was designed to build models from texture features to predict EGFR mutation status as well as differentiating mutations in exons 19 and 21. Another feature is that our cohort is composed of a heterogeneous population from North America compared to homogenous population from South East Asia in prior studies.[34-36] We also emphasized on robustness, stability, and reproducibility of the textural features and prediction models by employing LDA, LOOCV, and multivariate LR. The measurement of radiomic features over the entire tumor volume represents better tumor heterogeneity and is more accurate in comparison to single image with largest cross-sectional area.[37] Therefore, we sampled the entire cross-section of the tumor in multiple slices (3D), compared to contouring only the largest cross-sectional area of the lesion on single slice (2D) in the other studies.[36]

Evidence for a strong correlation between texture analysis and driver mutation in NSCLC, including *EGFR*, is limited.[16,34-36,38-42] Modest performance was demonstrated by combining clinical and radiomic features as risk factors for
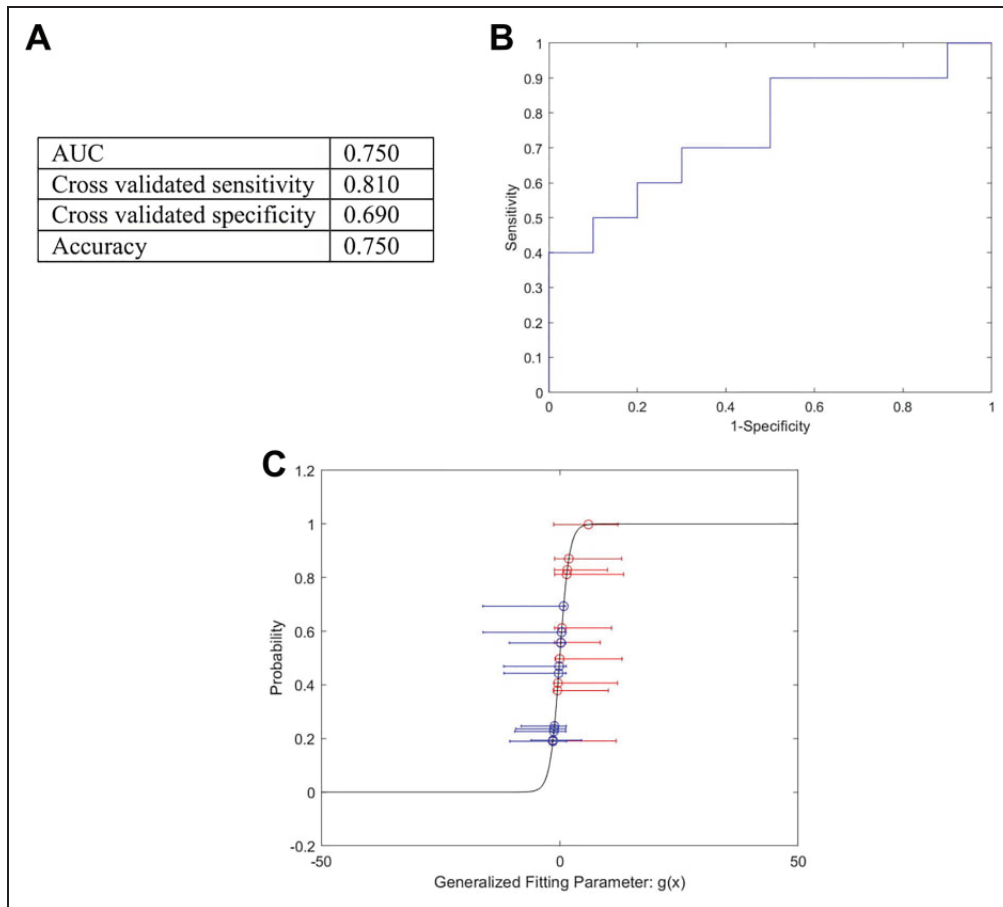
Figure 6. Comparison of point mutations in EGFR exon 19 and 21 in EGFR mutant-positive patients using CT Texture features. A, Tabulated results for the prediction of point mutations in EGFR exon 19 and 21 in EGFR mutant-positive patients with texture features derived from CT images. B, Corresponding receiver operator characteristic curve. C, Final multivariable logistic regression (computed tomography) model for point mutations in EGFR exon 19 and 21 in EGFR mutant-positive patients. Blue dots correspond to mutation in EGFR exon 21, while red dots imply EGFR exon 19 deletion. Error bars represent the standard deviation of the multivariable model response for each patient over all 100 bootstrap samples, on a 95% confidence interval. CT, computed tomography; EGFR, epidermal growth factor receptor.

EGFR mutation status and subtypes by Mei et al with AUC of 0.664 for *EGFR* mutation and 0.655 and 0.675 for exons 19 and 21 mutations, respectively.[34] In a retrospective study, combination of clinical history, standard imaging features, and radiomics with multivariable LR, and ROC analysis were utilized to predict histology and *EGFR* status.[37] Entropy and kurtosis were found to be the 2 most important radiomic features in distinguishing *EGFR* mutant from wild type. Comparison of the predictive performance of radiomics signature and CT morphological features for *EGFR* status by Tu et al demonstrated better performance for predicting *EGFR* mutant NSCLC than combined clinical and morphological features.[40] The CT and FDG-PET-CET texture features assessed in our study were found to have an improved AUC for the detection of an *EGFR* mutation (0.83 and 0.87, respectively) and improved AUC for the detection of the type of *EGFR* mutations (0.75 and 0.86, respectively) compared to the previous studies. The non-semantic textures features presented here improves the potential to predict the presence of an *EGFR* mutation by image analysis.

The limitations of our study include the retrospective nature of the analysis leading to patient selection bias and the relatively small sample size. Bootstrapping and other techniques were used to simulate different distributions of patient samples to overcome this shortcoming. However, stability and reproducibility of the textual features in our study need to be corroborated using a large prospective patient cohort in a multicenter study. Multi-class training of texture features was also not possible, so the analysis was limited to binary outcomes. As the study was retrospective in nature, imaging protocols were not standardized for all the patients resulting in different acquisition and reconstruction parameters. Extraction of texture would be significantly improved if a uniform data set is acquired. Although manual segmentation can be reliable, its reproducibility is questionable with available segmentation tools. However, automated segmentation software with high repeatability also has limitations in delineating margins in lesions with GGO. Finally, the genetic profiling was limited to the *EGFR* mutation and we did not analyze texture features

of other lung adenocarcinoma mutations, such as *ALK* and *KRAS* mutations.

Conclusion

In conclusion, the radiomics signature extracted from diagnostic CT and PET-CT images has potential as an imaging biomarker for noninvasively predicting *EGFR* mutations in NSCLC. Radiomic features from PET-CT imaging were more effective compared to CT imaging, both for identification of *EGFR* mutation and for differentiating between exon 19 and 21 mutations. However, an integrated model derived from CT morphological features, radiomics signature, and clinical data from a large prospective multicenter trial will be required to validate our findings and to embed this methodology in routine diagnostic care.

Appendix A

Definitions

GLCM (Gray-Level Co-Occurrence Matrix)

The GLCM functions characterize the texture of an image by calculating how often pairs of pixel with specific values and in a specified spatial relationship occur in an image,

GLRLM (Gray-Level Run Length Matrix)

The GLRLM quantifies gray level runs, which are defined as the length in number of pixels, of consecutive pixels that have the same gray level value.

NGTDM (Neighborhood Gray-Tone Difference Matrix)

A Neighboring Gray Tone Difference Matrix quantifies the difference between a gray value and the average gray value of its neighbors within distance.

LBP (Local Binary Pattern)

Local binary pattern is a type of visual descriptor for classification in computer vision. Local binary pattern measures the homogeneity of texture by determining the number of transitions from intensities higher than each central pixel to intensities lower than that central pixel.

References

1. Fintelmann FJ, Bernheim A, Digumarthy SR, et al. The 10 pillars of lung cancer screening: rationale and logistics of a lung cancer screening program. *Radiographics*. 2015;35(7):1893-1908.
2. Molina JR, Yang P, Cassivi SD, Schild SE, Adjei AA. Non-small cell lung cancer: epidemiology, risk factors, treatment, and survivorship. *Mayo Clin Proc*. 2008;83(5):584-594.
3. Kris MG, Johnson BE, Berry LD, et al. Using multiplexed assays of oncogenic drivers in lung cancers to select targeted drugs. *JAMA*. 2014;311(19):1998-2006.
4. Midha A, Dearden S, McCormack R. EGFR mutation incidence in non-small cell lung cancer of adenocarcinoma histology: a systematic review and global map by ethnicity (mutMapII). *Am J Cancer Res*. 2015;5(9):2892-2911.
5. Yang JC, Wu YL, Schuler M, et al. Afatinib versus cisplatin based chemotherapy for EGFR mutation-positive lung adenocarcinoma (LUX-Lung3 and LUX-Lung 6): analysis of overall survival data from two randomised, phase 3 trials. *Lancet Oncol*. 2015;16(2): 141-151.
6. Rosell R, Carcereny E, Gervais R, et al. Erlotinib versus standard chemotherapy as first-line treatment for European patients with advanced EGFR mutation-positive non-small-cell lung cancer (EURTAC): a multicentre, open-label, randomised phase 3 trial. *Lancet Oncol.* 2012;13(3):239-246.
7. Zhou C, Wu YL, Chen G, et al. Erlotinib versus chemotherapy as first-line treatment for patients with advanced EGFR mutation-positive non-small-cell lung cancer (OPTIMAL, CTONG-0802): a multicentre, open-label, randomised, phase 3 study. *Lancet Oncol.* 2011;12(8):735-742.
8. Fukuoka M, Wu YL, Thongprasert S, et al. Biomarker analyses and final overall survival results from a phase III, randomized, open-label, first-line study of gefitinib versus carboplatin/paclitaxel in clinically selected patients with advanced non-small-cell lung cancer in Asia (IPASS). *J Clin Oncol*. 2011;29(21):2866-2874.
9. Sequist LV, Yang JC, Yamamoto N, et al. Phase III study of afatinib or cisplatin plus pemetrexed in patients with metastatic lung adenocarcinoma with EGFR mutations. *J Clin Oncol*. 2013; 31(27):3327-3334.
10. Park K, Tan EH, O'Byrne K, et al. Afatinib versus gefitinib as first-line treatment of patients with EGFR mutation-positive non-small-cell lung cancer (LUX-Lung 7): a phase 2B, open-label, randomised controlled trial. *Lancet Oncol*. 2016;17(5):577-589.
11. Zhu J, Zhong W, Zhang G. Better survival with EGFR exon 19 than exon 21 mutations in gefitinib-treated non-small cell lung cancer patients is due to differential inhibition of downstream signals. *Cancer Lett*. 2008;265(2):307-317.
12. O'Connor JPB, Rose CJ, Waterton JC, Carano RA, Parker GJ, Jackson A. Imaging intratumor heterogeneity: role in therapy response, resistance, and clinical outcome. *Clin Cancer Res*. 2015;21(2):249-257.

13. Soria-Comes T, Palomar-Abril V, Ureste MM, Guerola MT, Maiques CM. Real-world data of the correlation between EGFR determination by liquid biopsy in non-squamous non-small cell lung cancer (NSCLC) and the EGFR profile in tumor biopsy [Published online March 7, 2019]. *Pathol Oncol Res*. 2019. doi:10.1007/s12253-019-00628-x.

14. Zhou JY, Zheng J, Yu ZF, et al. Comparative analysis of clinicoradiologic characteristics of lung adenocarcinomas with ALK rearrangements or EGFR mutations. *Eur Radiol*. 2015;25(5): 1257-1266.

15. Hsu JS, Huang MS, Chen CY, et al. Correlation between EGFR mutation status and computed tomography features in patients with advanced pulmonary adenocarcinoma. *J Thorac Imaging*. 2014;29(6):357-363.

16. Ozkan E, West A, Dedelow JA, et al. CT Gray-level texture analysis as a quantitative imaging biomarker of epidermal growth factor receptor mutation status in adenocarcinoma of the lung. *AJR Am J Roentgenol*. 2015;205(5):1016-1025.

17. Gillies RJ, Kinahan PE, Hricak H. Radiomics: images are more than pictures, they are data. *Radiology*. 2016;278(2):563-577.

18. Mazurowski MA. Radiogenomics: what it is and why it is important. *J Am Coll Radiol*. 2015;12(8):862-866.

19. Meyer M, Ronald J, Vernuccio F, et al. Reproducibility of CT radiomic features within the same patient: influence of radiation dose and CT reconstruction settings. *Radiology*. 2019;293(3): 583-591. doi:10.1148/radiol.2019190928.

20. Rosset A, Spadola L, Ratib O. OsiriX: an open-source software for navigating in multidimensional DICOM images. *J Digit Imaging*. 2004;17(3):205-216.

21. Solomon SB, Zakowski MF, Pao W, et al. Core needle lung biopsy specimens: adequacy for EGFR and KRAS mutational analysis. *AJR Am J Roentgenol*. 2010;194(1):266-269.

22. Masago K, Fujita S, Mio T, et al. Accuracy of epidermal growth factor receptor gene mutation analysis by direct sequencing method based on small biopsy specimens from patients with non-small cell lung cancer: analysis of results in 19 patients. *Int J Clin Oncol*. 2008;13(5):442-446.

23. Han HS, Lim SN, An JY, et al. Detection of EGFR mutation status in lung adenocarcinoma specimens with different proportions of tumor cells using two methods of differential sensitivity. *J Thorac Oncol*. 2012;7(2):355-364.

24. Lindeman NI, Cagle PT, Beasley MB, et al. Molecular testing guideline for selection of lung cancer patients for EGFR and ALK tyrosine kinase inhibitors: guideline from the College of American Pathologists, international association for the study of lung cancer, and association for molecular pathology. *J Thorac Oncol*. 2013;8(7):823-859.

25. Tabe-Bordbar S, Emad A, Zhao SD, Sinha S. A closer look at cross-validation for assessing the accuracy of gene regulatory networks and models. *Sci Rep*. 2018;8(1):6620.

26. DeLong ER, DeLong DM, Clarke-Pearson DL. Comparing the areas under two or more correlated receiver operating characteristic curves: a nonparametric approach. *Biometrics*. 1988;44(3):837-845.

27. Gevaert O, Echegaray S, Khuong A, et al. Predictive radiogenomics modeling of EGFR mutation status in lung cancer. *Sci Rep*. 2017;7:41674.

28. Chen Y, Yang Y, Ma L, et al. Prediction of EGFR mutations by conventional CT-features in advanced pulmonary adenocarcinoma. *Eur J Radiol*. 2019;112:44-51.

29. Lee HJ, Kim YT, Kang CH, et al. Epidermal growth factor receptor mutation in lung adenocarcinomas: relationship with CT characteristics and histologic subtypes. *Radiology*. 2013; 268(1):254-264.

30. Sabri A, Batool M, Xu Z, Bethune D, Abdolell M, Manos D. Predicting EGFR mutation status in lung cancer: proposal for a scoring model using imaging and demographic characteristics. *Eur Radiol*. 2016;26(11):4141-4147.

31. Zhou M, Leung A, Echegaray S, et al. Non-small cell lung cancer radiogenomics map identifies relationships between molecular and imaging phenotypes with prognostic implications. *Radiology*. 2018;286(1):307-315.

32. Zhang H, Cai W, Wang Y, Liao M, Tian S. CT and clinical characteristics that predict risk of EGFR mutation in non-small cell lung cancer: a systematic review and meta-analysis. *Int J Clin Oncol*. 2019;24(6):649-659.

33. Kim YI, Paeng JC, Park YS, et al. Relation of EGFR mutation status to metabolic activity in localized lung adenocarcinoma and its influence on the use of FDGPET/CT parameters in prognosis. *AJR Am J Roentgenol*. 2018;210(6):1346-1351.

34. Mei D, Luo Y, Wang Y, Gong J. CT texture analysis of lung adenocarcinoma: can features be surrogate biomarkers for EGFR mutation statuses. *Cancer Imaging*. 2018;18(1):52.

35. Tu W, Sun G, Fan L, et al. Radiomics signature: a potential and incremental predictor for EGFR mutation status in NSCLC patients, comparison with CT morphology. *Lung Cancer*. 2019; 132:28-35.

36. Li M, Zhang L, Tang W, Jin YJ, Qi LL, Wu N. Identification of epidermal growth factor receptor mutations in pulmonary adenocarcinoma using dual-energy spectral computed tomography. *Eur Radiol*. 2019;29(6):2989-2997.

37. Ng F, Kozarski R, Ganeshan B, Goh V. Assessment of tumor heterogeneity by CT texture analysis: can the largest cross-sectional area be used as an alternative to whole tumor analysis? *Eur J Radiol*. 2013;82(2):342-348.

38. Liu Y, Kim J, Balagurunathan Y, et al. Radiomic features are associated with EGFR mutation status in lung adenocarcinomas. *Clin LungCancer*. 2016;17(5):441-448.e6.

39. Sacconi B, Anzidei M, Leonardi A, et al. Analysis of CT features and quantitative texture analysis in patients with lung adenocarcinoma: a correlation with EGFR mutations and survival rates. *Clin Radiol*. 2017;72(6):443-450.

40. Digumarthy SR, Padole AM, Gullo R, Sequist LV, Kalra MK. Can CT radiomic analysis in NSCLC predict histology and EGFR mutation status? *Medicine (Baltimore)*. 2019;98(1): e13963.

41. Yip SS, Kim J, Coroller TP, et al. Associations between somatic mutations and metabolic imaging phenotypes in non-small cell lung cancer. *J Nucl Med*. 2017;58(4):569-576.

42. Park S, Ha S, Lee SH, et al. Intratumoral heterogeneity characterized by pretreatment PET in non-small cell lung cancer patients predicts progression-free survival on EGFR tyrosine kinase inhibitor. *PLoS One*. 2018;13(1):e0189766.